Surface profile measurement of low-frequency vibrating objects using temporal analysis of fringe pattern

C.J. Tay[a,*], C. Quan[a], Y. Fu[a], L.J. Chen[a], H.M. Shang[b]

[a]Department of Mechanical Engineering, National University of Singapore,

10 Kent Ridge Crescent, Singapore 119260, Singapore

[b]School of Mechanical and Production Engineering, Nanyang Technological University,

50 Nanyang Avenue, Singapore 639798, Sinagpore

* Corresponding author. Tel.: +65-874-2557; fax: +65-779-1459.

E-mail address: mpetaycj@nus.edu.sg (C.J. Tay)

Abstract

A simple and accurate algorithm (phase scanning method) is proposed for 3D surface contouring and dynamic response determination of a vibrating object. A sinusoidal fringe pattern is projected onto a low-frequency vibrating object by a programmable liquid crystal display projector. The fringe patterns are captured by a high-speed CCD camera with a telecentric gauging lens. Phase values are evaluated point by point using phase scanning method. From the phase values of each point on the object, the contour of the specimen at different instants of vibration can be retrieved. In this paper, a small vibrating coin is used to demonstrate the validity of the method and the experimental results are compared with test results on a stationary coin using four-step phase shifting and fast Fourier transform methods. The technique is especially useful in applications where the vibrating object has a complicated shape.

Keywords: Fringe projection; High-speed imaging; Dynamic response; Temporal phase analysis.

1. Introduction

Common optical methods for contouring include the use of holographic interferometry, moiré, fringe projection and other methods [1-13]. Among them, the fringe projection method is gaining grounds in many engineering applications. In the fringe projection technique, a known optical fringe pattern is projected onto the surface of interest; the distribution of the fringe pattern on the surface is perturbed in accordance with the profile of the test surface, thereby enabling direct derivation of surface profiles. Phase shifting techniques [14] are usually employed by projecting several fringe patterns with prescribed phase shift; however, these techniques are restricted to static objects. In many cases, 3D surface profiling is required for vibrating objects or for objects with continually changing profile.

With the availability of high-speed digital recording, it is now possible to record projected fringe pattern with rates exceeding 10,000 frames per second (fps). Recently several methods have been reported to retrieve the phase map from these images. Huang et al. [15] developed a color-encoded fringe projection technique to obtain the phase map by separating fringes with different colors followed by phase shifting. Previous investigations [16] have shown that fast Fourier transform (FFT) with carrier fringe method is another effective approach. It requires fringes with high spatial frequency acting as a carrier. With proper filtering in frequency domain, the contour can also be evaluated. These two approaches are based on a similar concept in getting the phase map in spatial coordinates along the time axis. Pawlowski et al. [17] developed a novel

approach to retrieve point-by-point phase values using 1D FFT along the time-axis. The spatial phase map at a certain instant can be obtained by combining the phase value of each point.

Unlike Pawlowski's method of 1D FFT, this paper presents a simple but robust technique to retrieve point-by-point phase values along the time-axis. This method utilizes a liquid crystal display (LCD) fringe projector and a high-speed CCD camera with telecentric gauging lens. High quality linear fringe patterns are projected on a vibrating object and the fringe patterns are imaged consecutively by a high-speed CCD camera. Applying phase scanning method [18] on these fringe patterns, the surface profile at any instant, as well as the amplitude and frequency of the vibration, can be reconstructed.

2. Theoretical analysis

Fig. 1 shows the schematic layout of the projection and imaging system. With normal viewing, the phase change φ due to height h is given by

$$h = \frac{L}{d} S = \frac{L}{d} \frac{\varphi}{2\pi f_0} = k\varphi , \tag{1}$$

where L is the distance between the LCD projector and the reference plane, d is the distance between the projector and camera axis, f_0 is the spatial frequency of the projected fringes on the reference plane and k, which can be obtained by calibration, is an

optical coefficient related to the configuration of the system. φ is the phase angle change which contains the surface height information.

When a vertical sinusoidal fringe pattern is projected onto a vibrating 3D object surface, the distribution of the grating is perturbed by two factors, the vibration or deformation of the specimen and the initial profile of the test surface. The mathematical representation of the intensity distribution captured by a CCD camera is governed by the following equation:

$$I(x,y,t) = a(x,y,t) + b(x,y,t) \times \cos[2\pi f_0 x + \varphi_0(x,y) + \varphi(x,y,t)], \quad (2)$$

where $a(x,y,t)$ and $b(x,y,t)$ are the background and modulation factor, respectively, $\varphi_0(x,y)$ is an initial phase which contains the shape information, and $\varphi(x,y,t)$ is a time-dependent phase function related to the object vibration or deformation. $a(x,y,t)$ and $b(x,y,t)$, which are also functions of time, are both slowly varying functions. Hence, $a(x,y,t)$ and $b(x,y,t)$ can be regarded as constants in one period of intensity change.

If the amplitude of the vibration is large enough, the variation of $\varphi(x,y,t)$ will be higher than 2π, which implies more than one period intensity change. In most cases, this assumption can be satisfied by proper selection of carrier fringe frequency, projection angle and imaging area. With this assumption, the detectable maximum and minimum values of intensity within one period of intensity change at a certain point P (x_p, y_p) on the test surface can be written as

$$I_{\max}(x_p, y_p) = a(x_p, y_p) + b(x_p, y_p), \tag{3}$$

$$I_{\min}(x_p, y_p) = a(x_p, y_p) - b(x_p, y_p). \tag{4}$$

Subsequently Eq. (2) is rewritten as

$$I(x_p, y_p, t) = \frac{1}{2}[I_{\max}(x_p, y_p) + I_{\min}(x_p, y_p)] + \frac{1}{2}[I_{\max}(x_p, y_p) - I_{\min}(x_p, y_p)]\cos\phi_p(x_p, y_p, t), \tag{5}$$

where

$$\phi_p(x_p, y_p, t) = 2\pi f_0 x_p + \phi_0(x_p, y_p) + \varphi(x_p, y_p, t). \tag{6}$$

Hence the phase value can be expressed as

$$\phi_p(x_p, y_p, t) = \arccos\left[\frac{2I(x_p, y_p, t) - I_{\max}(x_p, y_p) - I_{\min}(x_p, y_p)}{I_{\max}(x_p, y_p) - I_{\min}(x_p, y_p)}\right]. \tag{7}$$

As the first two terms in Eq. (6) are constants on the time-axis, the relative phase variation due to vibration or deformation at point *P* can be obtained as

$$\varphi(x_p, y_p, \Delta t) = \phi_p(x_p, y_p, t_2) - \phi_p(x_p, y_p, t_1). \tag{8}$$

At a certain time T, the phase map representing the contour of the specimen can be expressed as

$$\phi(x, y, T) = 2\pi f_0 x + \phi_0(x, y) + \varphi(x, y, T), \tag{9}$$

where $\varphi(x, y, T)$ denotes the phase which is related to the vibration amplitude or deformation at instant T.

Both phases $\varphi(x_p, y_p, \Delta t)$ and $\phi(x, y, T)$ are wrapped phase values, as $\phi_p(x_p, y_p, t)$ given by Eq. (7) is within 0 to π. For unwrapping, the values of ϕ at each point are converted from $[0, \pi]$ to $[0, 2\pi]$. The phase values after conversion are determined by two factors, namely direction of vibration or deformation and the slope of intensity $\frac{\partial I}{\partial t}$ along the time-axis. Table 1 shows the details of the conversion. Unwrapping the phase values $\varphi(x_p, y_p, \Delta t)$ given by Eq. (8) along the time-axis is a 1D problem; retrieving the continuous phase values from $\phi(x, y, T)$ in Eq. (9) is a 2D unwrapping problem where numerous unwrapping algorithms are applicable [19].

3. Experimental illustration

The experimental setup is shown in Fig. 2. A coin of 21 mm diameter and having a diffuse surface is subjected to a vibration with different amplitudes using a vibrator. The frequency of vibration is controlled by a function generator. A vertical sinusoidal fringe pattern is projected onto the object by a programmable LCD projector. The fringe patterns are captured at right angle by a high speed CCD camera (KODAK Motion

Corder Analyzer, SR-Ultra) with a telecentric gauging lens (MELLES GRIOT 59LGH416). Magnification of telecentric lens, unlike conventional lenses, is independent of the working distance. It remains constant regardless of the object distance from the camera. This reduces magnification error due to the vibration and greatly extends gauging depth of field. Fig. 3 shows the difference between the telecentric lens and a conventional lens. With the special lens, the positions of a vibrating object in the image plane remain the same, while only the fringe pattern is shifted periodically. The pitch of the fringe pattern and the angle of projection are selected according to the amplitude of vibration such that the phase variation in one cycle of vibration is more than 2π .

4. Results and discussion

Fig. 4(a) shows an image of the initial test object before fringe projection. A small area of interest containing 256 ×256 pixels is shown in Fig. 4(b). The coefficient k in Eq. (1) can be calibrated by shifting the object through a known distance in the z-axis and the corresponding phase difference on the specimen is determined by the conventional four-step phase shifting method. Using Eq. (1), the value of k is evaluated to be 0.8692 mm/rad. The test object is subjected to a triangular wave vibration with a frequency of approximately 6 Hz. Fringe patterns are recorded at intervals of 0.004 s with a camera recording rate of 250 fps. Fig. 5 shows typical fringe patterns captured by the high-speed CCD camera at different moments. Five hundred images can be captured during a 2-s period. Among them, 90 consecutive images are selected for processing. Within these 90 images, four images representing extreme positions of vibration are identified; subsequently the direction of vibration can be determined. The extreme positions of

vibration are readily identified by the computer since the first derivative of intensity ($\frac{\partial I}{\partial t}$) of most pixels in the image changes sign (either from positive to negative or vice versa).

For each pixel, ninety data points along the time axis are obtained. Fig. 6(a) shows the gray value variation of point A (indicated in Fig. 4b). The extreme positions of vibration are indicated as shown in Fig. 6(a). The wrapped phase values are presented in Fig. 6(b). After unwrapping along the time-axis, the continuous phase profile, as shown in Fig. 6(c), can be obtained. The frequency of vibration is evaluated as 5.68 Hz, and the amplitude of phase change A_ϕ is 13.12 rad. Consequently the amplitude of the vibration is calculated as 11.40 mm. Fig. 7 shows the gray value variation, wrapped phase map and continuous phase profile of point B (indicated in Fig. 4b), when the specimen is vibrated sinusoidally with frequency of 4.55 Hz and amplitude of 13.02 mm.

From Figs. 6(a) and 7(a), it can be observed that the maximum and minimum values of each cycle of phase variation (2π change) are slightly different. This is due to fluctuation of the LCD panel and intensity of the projector light source. Relatively large errors in the phase profile also occur when the gray value approaches the extreme values. The errors are introduced by (1) the maximum or minimum values detected by the camera are slightly different from the actual extreme gray scale values and (2) for a sine-wave configuration, a slight difference in gray level near the extreme values causes a large change in phase value. The errors can be minimized by proper selection of the recording rate and frequency of the carrier fringes such that the number of sampling points is optimized within one cycle of gray level change. In this study, it is found that 10-16 frames per cycle produce the best results.

At a certain instant, a combination of phase values on each pixel produces a wrapped spatial phase map as shown in Fig. 8(a). After unwrapping, the continuous phase map, which represents the surface profile, can be obtained. Fig. 8(b) shows the continuous phase map of the object surface. Using the calibrated coefficient *k*, the phase map can be converted into a 3D surface profile as shown in Fig. 8(c). Some vertical stripes are observed on the phase map, this is due to the errors introduced by the extreme values of gray level mentioned above. In spatial coordinate, these errors can be reduced by applying a filtering mask on the phase map. In this application, a 3×3 median mask is used.

To verify the accuracy of the proposed method, a comparison is made with the fast Fourier transform (FFT) and conventional four-step phase shifting methods [14]. Four fringe patterns with a phase increment of $\pi/2$ are projected onto a stationary test coin using the same experimental setup. For each fringe pattern, an averaged image is obtained from 500 images. Four of such images are subsequently used in the four-step phase shifting algorithm, while one of the images is used for the FFT method. Figs. 9(a), (b), and (c) show respectively, the phase maps obtained by the phase scanning, FFT and phase shifting methods. As the phase evaluation is carried out point-by-point along the time-axis, the phase scanning method is best suited to determination of a surface with a complicated profile. As can be seen, the result from the phase scanning method (Fig. 9a) shows a better image quality than the FFT method (Fig.9b), especially at the top half of the image. The results from the phase shifting method (Fig. 9c) show similar image quality with the phase scanning method. However, as mentioned above, images for the phase shifting method are obtained on the object while at rest. Fig. 10 shows a

comparison of the phase profile on cross-section C-C (indicated in Fig. 4b) between the phase scanning and phase shifting methods. It is shown that the phase profiles obtained by the two methods agree well. The maximum difference of the phase value between two methods is 0.012 rad, which denotes a height difference of 0.01 mm.

It is worth noting that using the proposed technique, measurement is limited to out-of-plane displacement, and high quality sinusoidal fringes are required to identify the maximum and minimum gray values. The recording rate of the camera should also be higher than the frequency of vibration. In this application, a recording rate of at least 10 times the vibration frequency is found adequate.

5. Concluding remarks

This paper presents a new method to retrieve the surface profile from a slow vibrating object using fringe projection technique. Unlike conventional phase evaluation techniques, this method analyses the phase values point-by-point along the time axis. High quality surface profiles can be retrieved from a vibrating object, where normal phase-shifting methods are not applicable. Accuracy in profile measurement is up to 1/500 of the vibrating amplitude. With further development, the algorithm may be extended to other optical techniques, such as moiré interferometry, electronic speckle pattern interferometry (ESPI) and digital speckle shearing interferometry (DSSI) for the study of dynamic problems.

References

1. Yatagai T, Idesawa M. Automatic fringe analysis for moiré topography. Opt Laser Eng 1982;3:73-83.
2. Dai YZ, Chiang FP. Contouring by moiré interferometry. Exp Mech 1991;31:76-81.
3. Hovanesian JD, Hung YY. Moire contour-sum contour difference, and vibration analysis of arbitrary objects. Appl Opt 1971;10:2734.
4. Thalmann R, Dandliker R. Holographic contouring using electronic phase measurement. Opt Eng 1985; 24(6):930-5.
5. Quan C, Shang HM, Tay CJ, Bryanston-Cross PJ. Holographic contouring using double-source technique and Fourier transform analysis. Opt Laser Eng 1998; 30: 351-62.
6. Rastogi PK. Visualisation of the contours of equal slope of an arbitrarily-shaped object using holographic moiré. Opt Eng 1994; 33(7):2373-7.
7. Takeda M, Mutoh K. Fourier transform profilometry of 3-D diffuse objects by spatial phase detection. Appl Opt 1986; 25(10):1630-3.
8. Suganuma M, Yoshizawa T. Three-dimensional shape analysis by use of a projected grating image. Opt Eng 1991; 30(10):1529-33.
9. Kalm MK, Juptner W, Osten W. Automatic adaption of projected fringe pattern using a programmable LCD-projector. Proc SPIE 1997; 3100:156-65.
10. Halioua M, Liu HC. Optical three-dimensional sensing by phase measuring profilometry. Opt Laser Eng 1989; 11(3):185-215.

11. Su XY, Zhou WS. Automated phase-measuring profilometry using defocused projection of a Ronchi grating. Opt Commun 1992; 94:561.
12. Pedrini G, Schedin S, Tiziani HJ. Pulsed digital holography combined with laser vibrometry for 3D measurements of vibrating objects. Opt Laser Eng 2002;38:117-29.
13. Chen F, Brown GM, Song M. Overview of three-dimensional shape measurement using optical methods. Opt Eng 2000; 39(1):10-22.
14. Quan C, He XY, Tay CJ, Shang HM. 3D surface profile measurement using LCD fringe projection. Proc SPIE 2001; 4317: 511-6.
15. Huang PS, Hu Q, Jin F, Chiang FP. Color-encoded digital fringe projection for high-speed three-dimensional surface contouring. Opt Eng 1999; 38(6):1065-71.
16. Tay CJ, Quan C, Shang HM, Wu T, Wang SH. New method for measuring dynamic response of small components by fringe projection. Opt Eng 2003;42(6):1715-20
17. Pawlowski ME, Kujawinska M, Wegiel MG. Shape and motion measurement of time-varying three-dimensional objects based on spatiotemporal fringe-pattern analysis. Opt Eng 2002; 41(2): 450-9.
18. Li X, Tao G, Yang Y. Continual deformation analysis with scanning phase method and time sequence phase method in temporal speckle pattern interferometry. Opt Laser Technol 2001; 33:53-9.
19. Ghiglia DC, Pritt MD. Two-dimensional phase unwrapping, theory, algorithms, and software. New York: Wiley; 1998.

List of Table

List of Figures

Table 1

Phase Value in $[0,\ \pi]$	Direction of Vibration or Deformation	Slope of Intensity along Time Axis $\frac{\partial I}{\partial t}$	Phase Value in $[0,\ 2\pi]$ after conversion
ϕ	Forward	≥ 0	$2\pi - \phi$
		< 0	ϕ
	Backward	≥ 0	ϕ
		< 0	$2\pi - \phi$

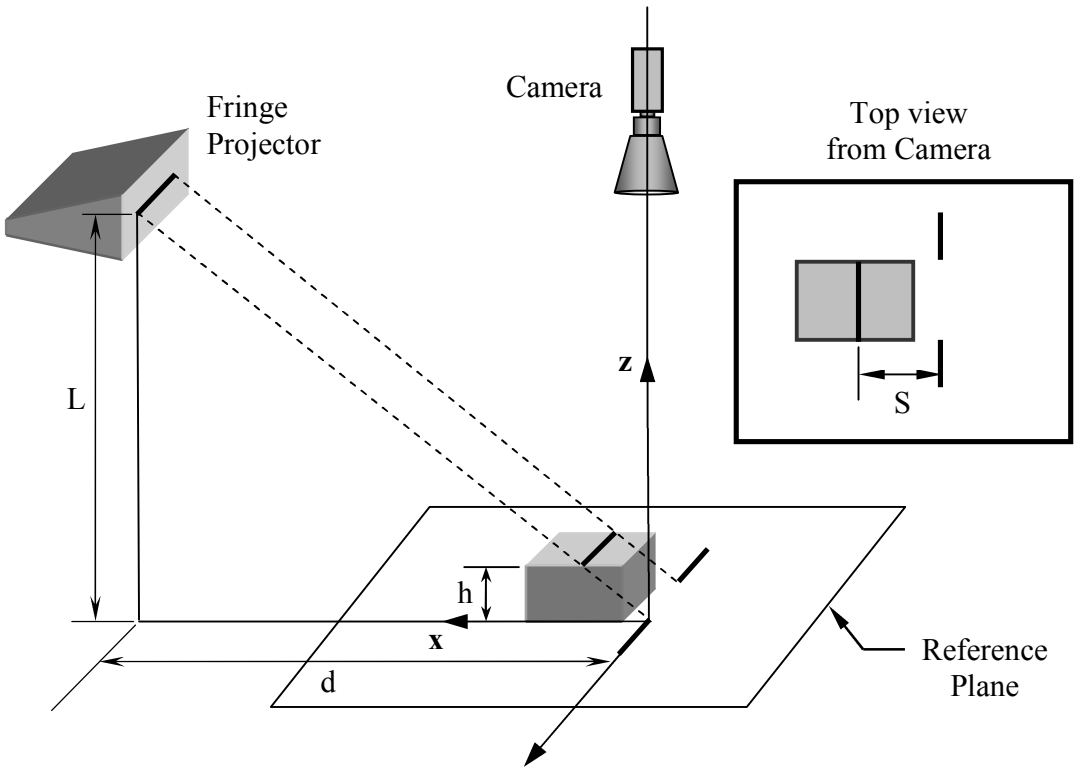
Fringe
Projector
Camera
Top view
from Camera
z
L
S
h
x
d
Reference
Plane

Figure 1

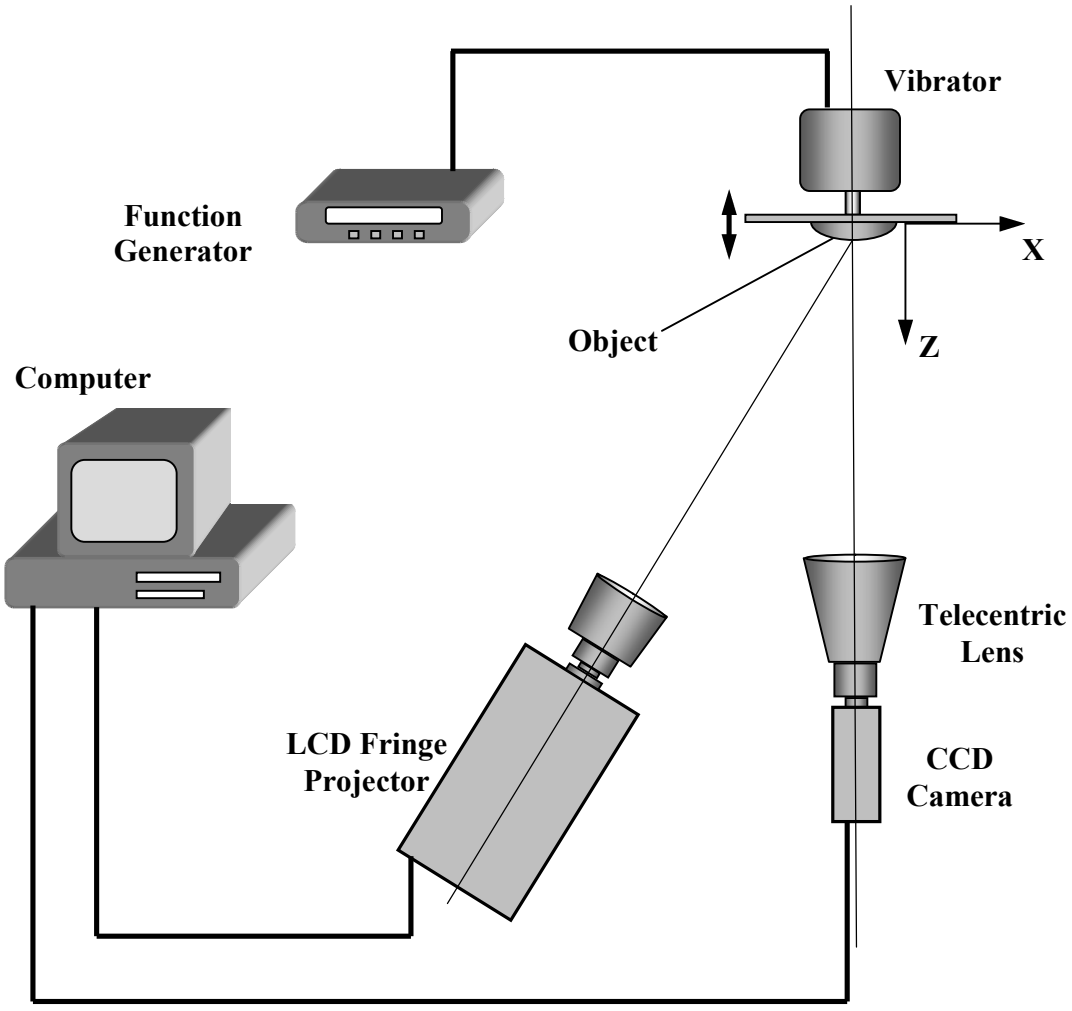
Vibrator
Function
Generator
X
Object
Z
Computer
Telecentric
Lens
LCD Fringe
Projector
CCD
Camera

Figure 2

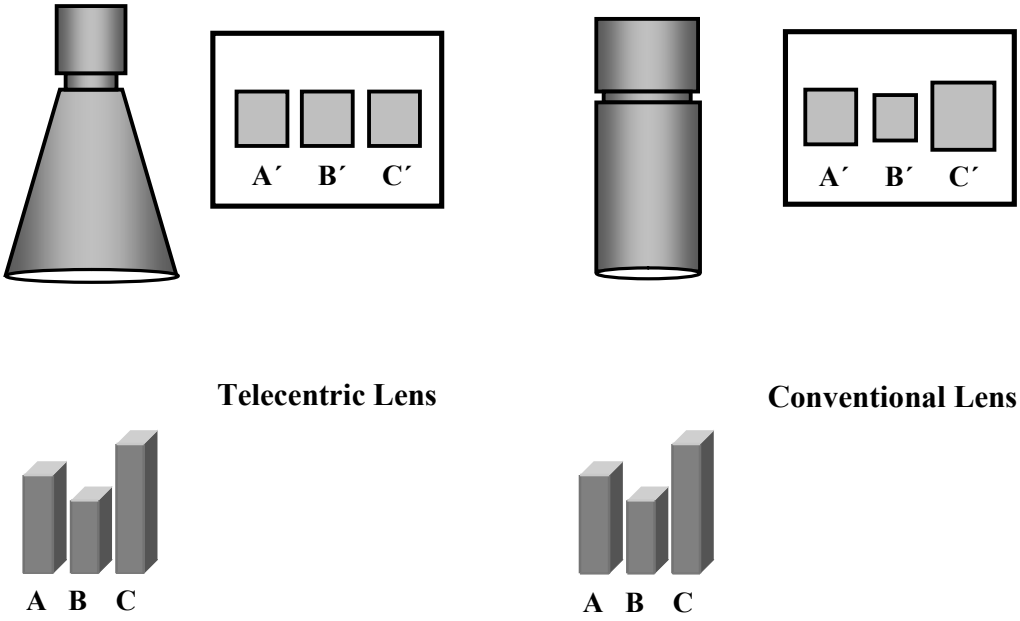

Figure 3

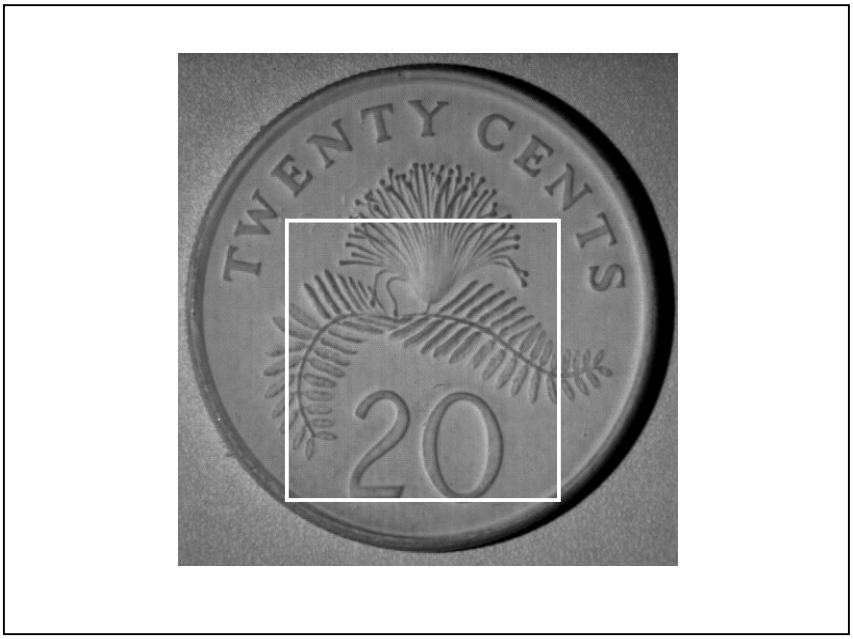

(a)

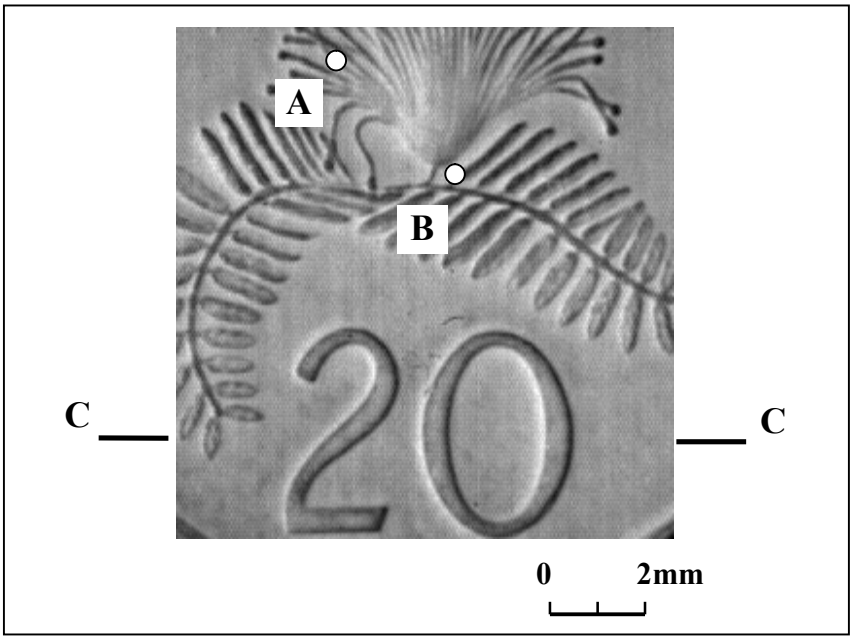

(b)

Figure 4

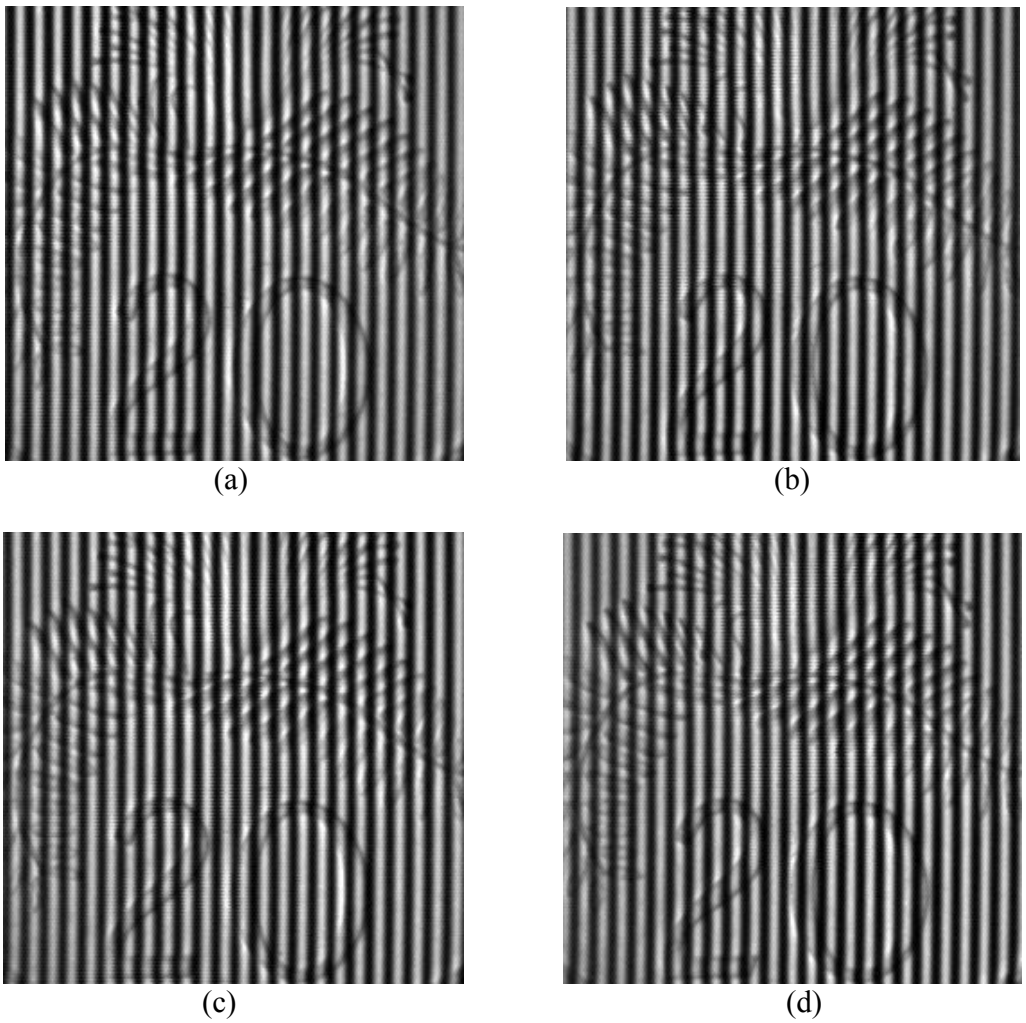

Figure 5

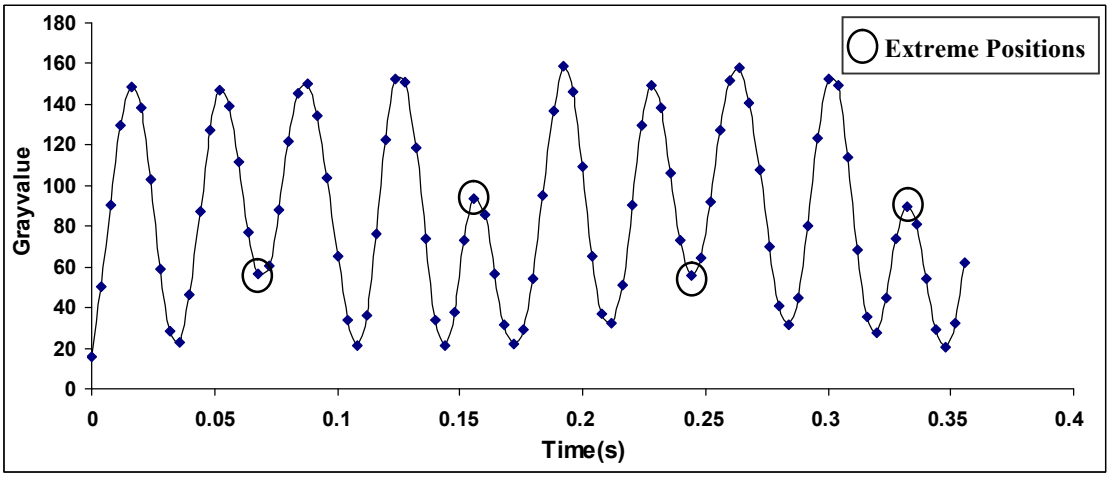
Extreme Positions
Grayvalue
Time(s)
0
20
40
60
80
100
120
140
160
180
0.05
0.1
0.15
0.2
0.25
0.3
0.35
0.4

(a)

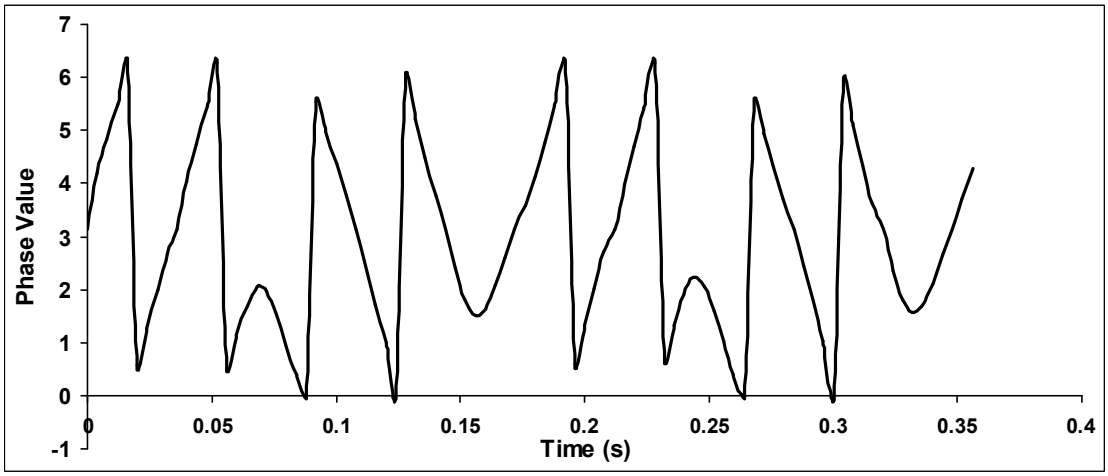
Phase Value
Time (s)
-1
0
1
2
3
4
5
6
7
0.05
0.1
0.15
0.2
0.25
0.3
0.35
0.4

(b)

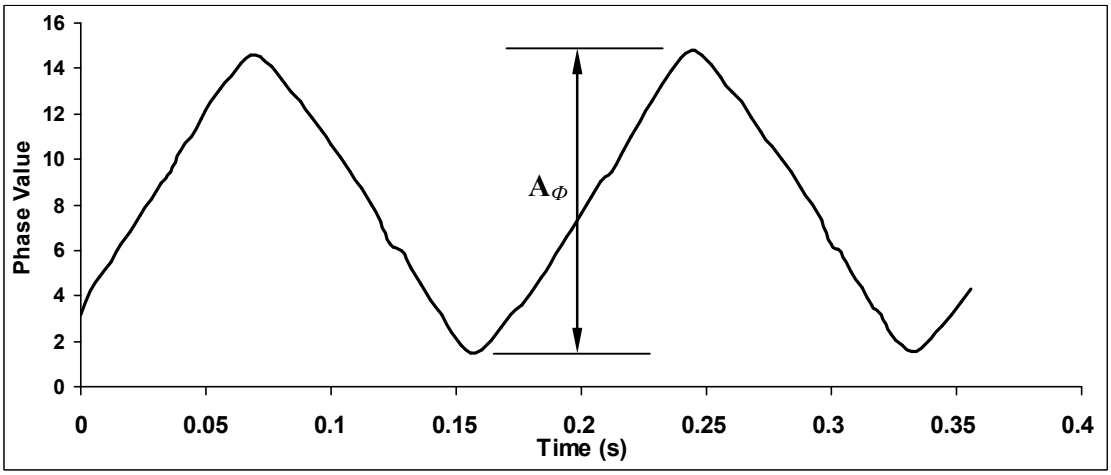
Phase Value
Time (s)
A_Φ
0
2
4
6
8
10
12
14
16
0.05
0.1
0.15
0.2
0.25
0.3
0.35
0.4

(c)

Figure 6

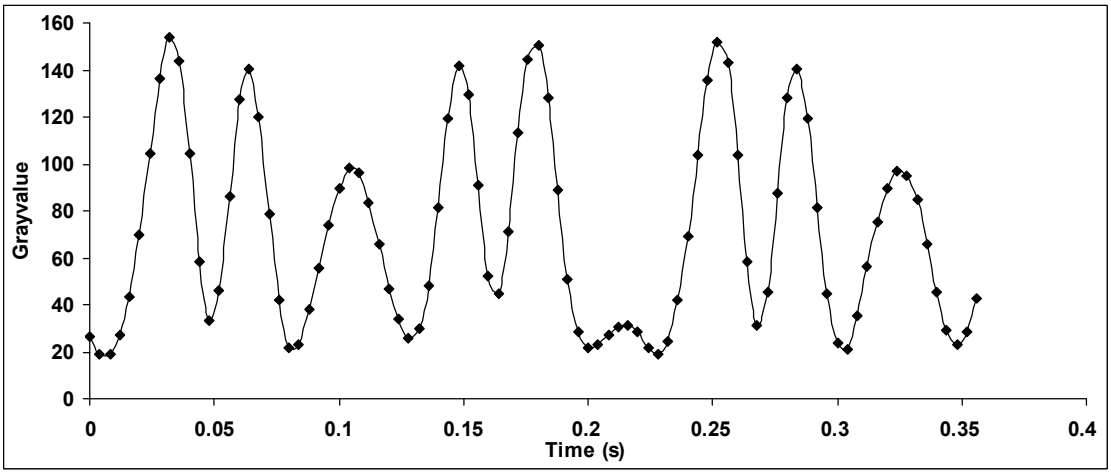
Grayvalue
160
140
120
100
80
60
40
20
0
0
0.05
0.1
0.15
0.2
0.25
0.3
0.35
0.4
Time (s)

(a)

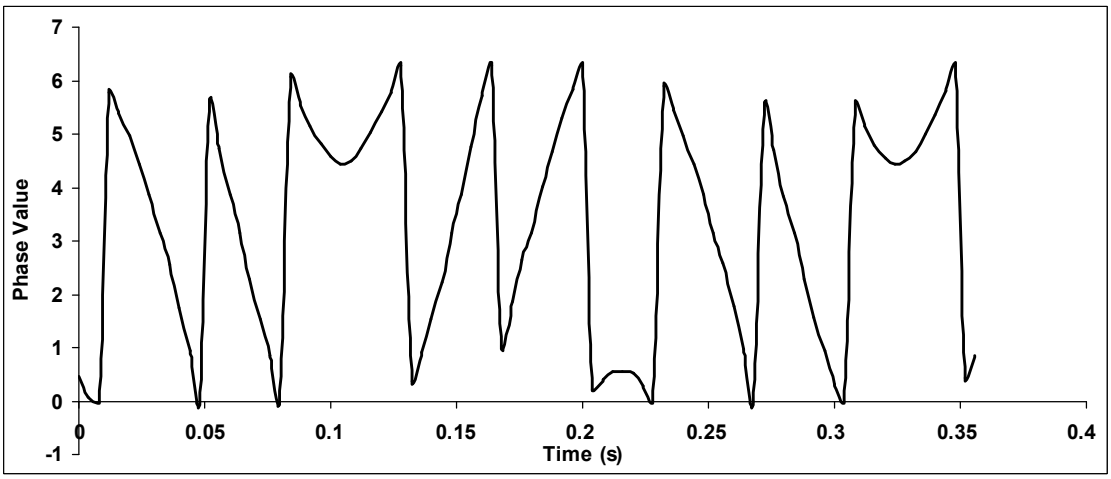
Phase Value
7
6
5
4
3
2
1
0
-1
0
0.05
0.1
0.15
0.2
0.25
0.3
0.35
0.4
Time (s)

(b)

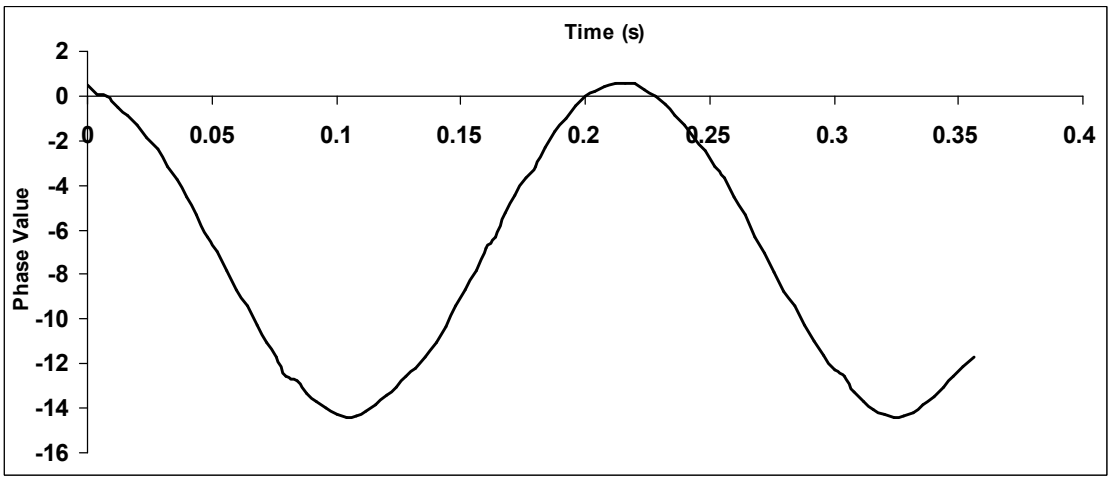
Time (s)
Phase Value
2
0
-2
-4
-6
-8
-10
-12
-14
-16
0
0.05
0.1
0.15
0.2
0.25
0.3
0.35
0.4

(c)

Figure 7

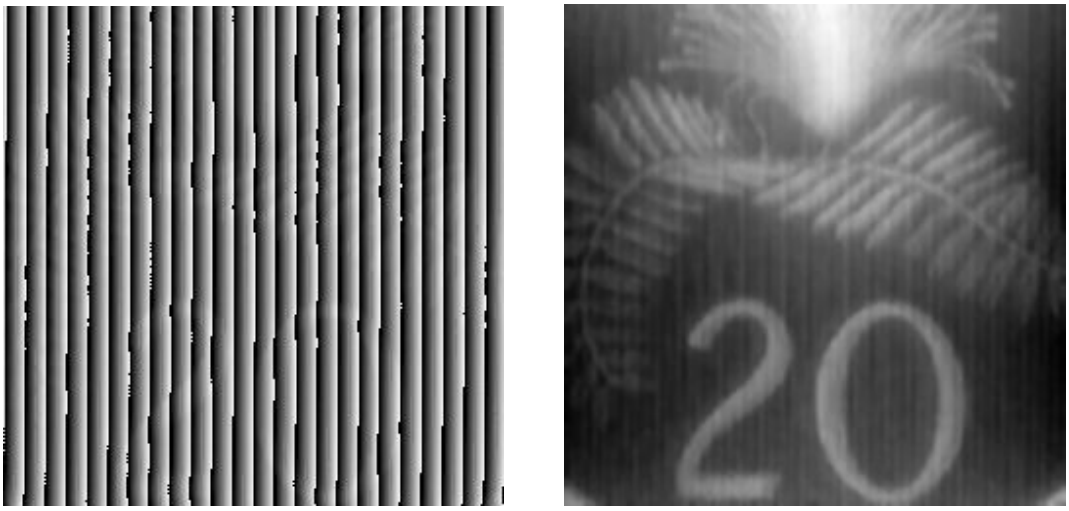

(a) (b)

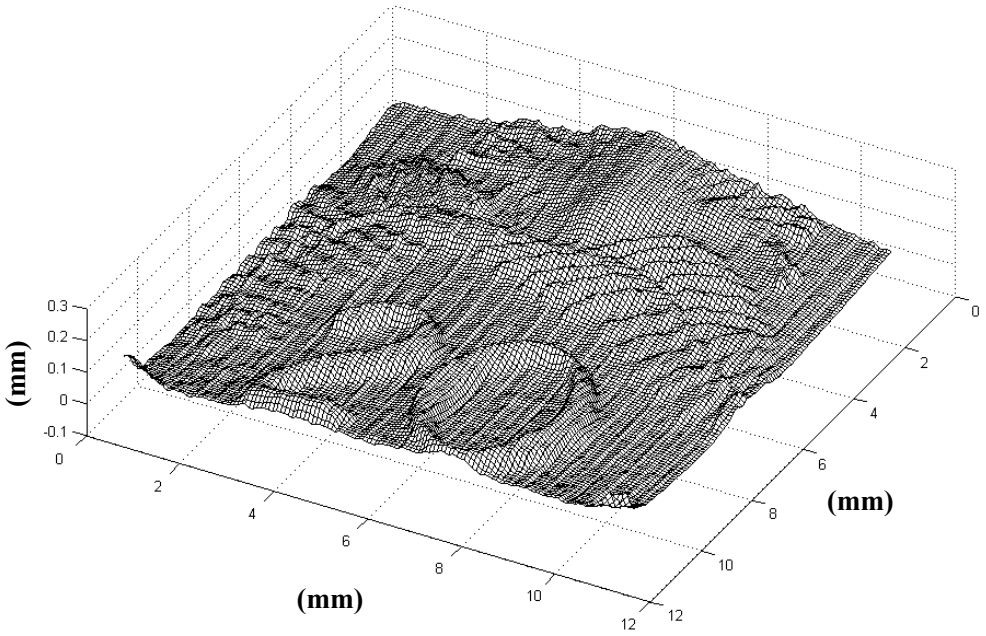

(c)

Figure 8

(a)

(b)

(c)

Figure 9

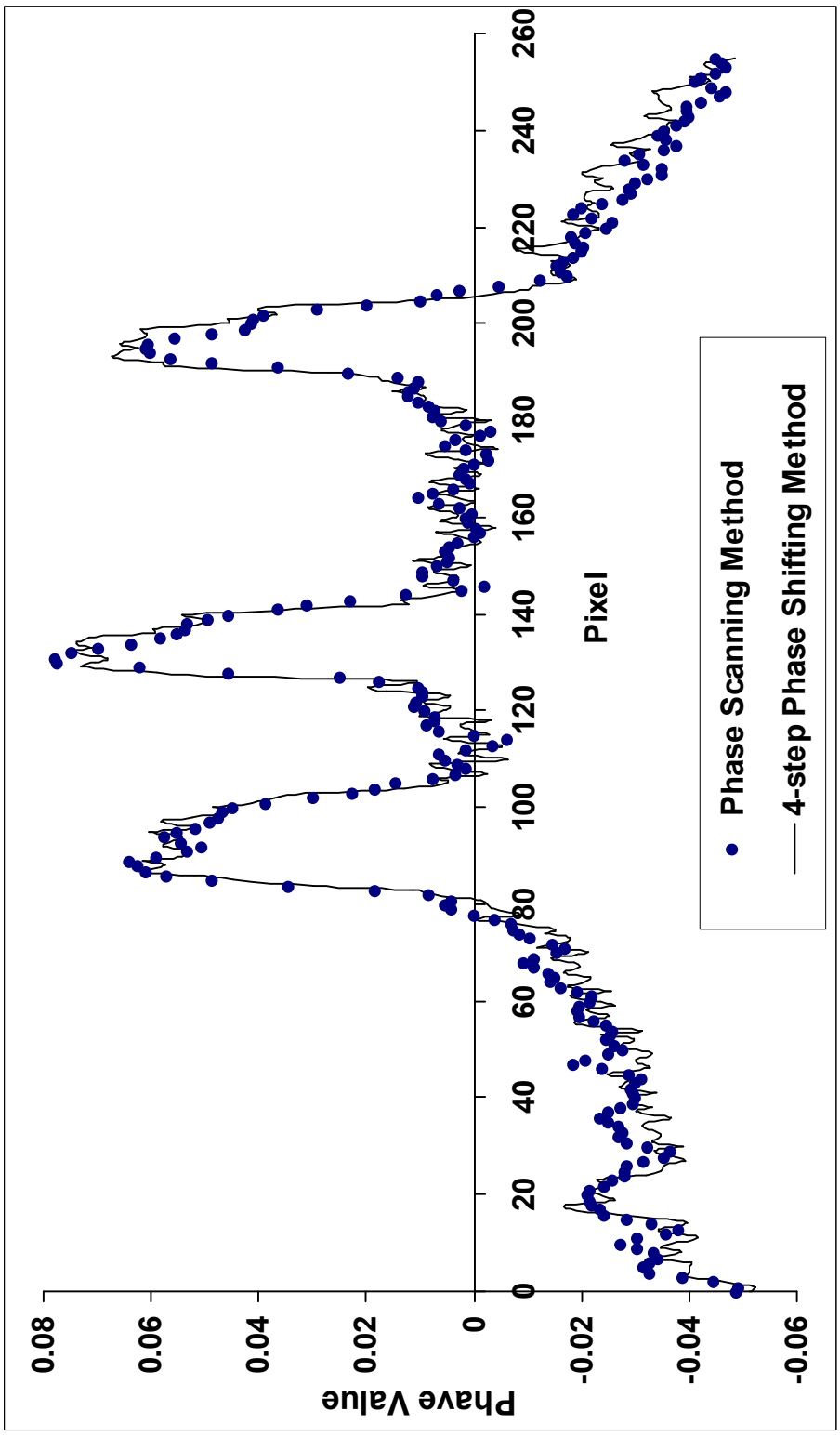
Phase Scanning Method
4-step Phase Shifting Method
Pixel
Phave Value
0.08
0.06
0.04
0.02
0
-0.02
-0.04
-0.06
0
20
40
60
80
100
120
140
160
180
200
220
240
260

Figure 10